PHYSICAL REVIEW D

PARTICLES AND FIELDS

THIRD SERIES, VOLUME 36, NUMBER 11 1 DECEMBER 1987

Limits on $\nu_\mu \rightarrow \nu_\tau$ and $\nu_\mu \rightarrow \nu_e$ oscillations

J. Bofill,[a] W. Busza, T. Eldridge,[b] J. I. Friedman, S. Fuess, M. C. Goodman,[c] H. W. Kendall, T. Lyons, R. Magahiz,[d] T. Mattison, A. Mukherjee,[a] L. S. Osborne, R. Pitt,[e] L. Rosenson, A. Sandacz,[f] M. Tartaglia,[g] F. E. Taylor, R. Verdier, S. Whitaker,[h] and G. P. Yeh[a]

Massachusetts Institute of Technology, Cambridge, Massachusetts 02139

D. Bogert, R. Burnstein,[i] J. G. Morfin, L. Stutte, and J. K. Walker[j]

Fermi National Accelerator Laboratory, Batavia, Illinois 60510

M. Abolins, R. Brock, A. Cohen,[k] J. Ernwein,[l] D. Owen, J. Slate,[b] and H. Weerts

Michigan State University, East Lansing, Michigan 48824

(Received 12 February 1987; revised manuscript received 24 August 1987)

Limits on $\nu_\mu \rightarrow \nu_\tau$ and $\nu_\mu \rightarrow \nu_e$ neutrino oscillations have been determined using a massive fine-grained calorimeter exposed to a narrow-band neutrino beam at Fermilab. We have searched for neutrino-oscillation candidates by selecting events with the quasielastic topology. By having a visible energy which is predominantly in the lepton sector, this type of event has sensitivity to neutrino oscillations and a signature which is indicative of the incident neutrino flavor. From cuts on the event energy allowed by the properties of the incident narrow-band beam, we have determined the following limits at the 90% confidence level for the neutrino-mass-squared difference Δm^2 at maximum mixing: $\nu_\mu \rightarrow \nu_\tau$, $\Delta m^2 < 10.2$ eV^2; $\bar{\nu}_\mu \rightarrow \bar{\nu}_\tau$, $\Delta m^2 < 6.5$ eV^2; $\nu_\mu \rightarrow \nu_e$, $\Delta m^2 < 1.8$ eV^2; and $\bar{\nu}_\mu \rightarrow \bar{\nu}_e$, $\Delta m^2 < 3.1$ eV^2. In the limit where Δm^2 becomes large we have found the mixing angle θ satisfies the following limits at the 90% confidence level: for $\nu_\mu \rightarrow \nu_\tau$, $\sin^2 2\theta < 0.34$; for $\bar{\nu}_\mu \rightarrow \bar{\nu}_\tau$, $\sin^2 2\theta < 0.15$; $\nu_\mu \rightarrow \nu_e$, $\sin^2 2\theta < 0.015$; and for $\bar{\nu}_\mu \rightarrow \bar{\nu}_e$, $\sin^2 2\theta < 0.04$.

I. INTRODUCTION

Several properties of the neutrino remain undetermined even after roughly 30 years of experimentation. The basic question concerning the *CP* structure of the neutrino remains unanswered—whether the neutrino is a Majorana or a Dirac particle. Possible mixing of neutrinos belonging to different lepton families remains a possibility. Given the fundamental nature of these questions, it is important to gather more data on the mass and possible mixing of different neutrino flavors.

If the neutrino has a finite mass and if there are finite differences between the masses of neutrinos of unlike flavors, there can be neutrino flavor mixing. Thus, a beam initially composed of only one neutrino flavor can become a mixture of flavors determined by the neutrino-mass-squared difference, the mixing angle, the propagation distance, and the beam energy. Limits on the occurrence of this neutrino mixing can lead to very sensitive constraints on mass differences between neutrino species. In the case of mixing between only two neutrino species,[1] the probability that an initial neutrino species i with mass eigenvalue m_i oscillates into a neutrino species j with mass eigenvalue m_j is given by[2,3]

$$P(\nu_i \rightarrow \nu_j) = \sin^2(2\theta)\sin^2(1.27\Delta m^2_{ij} L/E_\nu) , \quad (1)$$

where $\Delta m^2_{ij} = |m_i^2 - m_j^2|$ in eV^2, L is the distance from the neutrino source in kilometers, E_ν is the neutrino energy in GeV, and θ is an unknown mixing angle. In this experiment we have determined an upper limit for the probability of the neutrino flavor oscillations $P(\nu_\mu \rightarrow \nu_\tau)$ and $P(\nu_\mu \rightarrow \nu_e)$. We use these upper limits to exclude regions in the Δm^2 vs $\sin^2(2\theta)$ plane.[4] The $L/\langle E_\nu \rangle$ region of this experiment is roughly 0.023 km/GeV.

Two experimental techniques have been used to detect the presence of neutrino oscillations. In the first technique a search is made for a discrepancy in the measured neutrino flux using detectors located at various distances from the neutrino source, or for a difference between the measurement and the expected neutrino flux in a single detector. Such a "disappearance" experiment typically involves minimal final-state identification. A detailed

understanding of the incident neutrino flux is necessary to obtain a good limit. The second technique involves the attempt to detect the anomalous presence of a given neutrino species in a beam of known composition. This type of "appearance" experiment necessarily requires significant final-state discrimination to signal the appearance of a different neutrino flavor in a beam of known composition.

The data in this study were collected with the neutrino detector located in Laboratory C at Fermilab during a narrow-band beam run. The neutrino detector was designed to measure neutral-current interactions,[5–7] but with its high modularity it can also detect and measure the kinematics of quasielastic neutrino-nucleon scattering events. By imposing kinematic constraints allowed by the incident narrow-band neutrino beam, a direct separation of the oscillation-candidate events from background events was performed and limits on neutrino oscillations were determined.

The selection of quasielastic events in a narrow-band beam has the advantage of minimizing the visible energy in the hadronic sector of the neutrino interaction. While the hadronic energy spectrum may vary from flavor to flavor because of flavor-dependent form factors, the whole range of hadronic energy is expected to be no more than a few hundred MeV (Ref. 8). Thus, we searched for neutrino oscillations with final states which could have resulted from any of the following three reaction chains.

Case A: ν_μ oscillation into ν_τ. The ν_τ undergoes a quasielastic interaction $\nu_\tau n \rightarrow \tau^- p$, followed by the decay $\tau^- \rightarrow \mu^- \bar{\nu}_\mu \nu_\tau$ [see Fig. 1(a)].

Case B: ν_μ oscillation into ν_τ. The ν_τ interacts quasielastically with the nucleon by the reaction $\nu_\tau n \rightarrow \tau^- p$, followed by the decay $\tau^- \rightarrow e^- \bar{\nu}_e \nu_\tau$ [see Fig. 1(a)].

Case C: ν_μ oscillation into ν_e. The ν_e scatters via the quasielastic channel $\nu_e n \rightarrow e^- p$ [see Fig. 1(b)].

For each of the three reaction chains described above the antineutrino case was also considered.

In cases A and B we searched for a single muon or electron, respectively, with an event energy significantly smaller than the narrow-band beam energy. In case C a search is made for a single electromagnetic shower with an energy consistent with the spectrum of the narrow-band beam. This clean event topology, with the straightforward candidate event selection according to missing energy, enabled the systematic errors of this search to be well controlled and the upper bounds on the various neutrino flavor oscillations to be directly estimated.

A brief description of the experimental apparatus is given in Sec. II. Section III describes the data analysis. Section IV gives the oscillation upper limits. Section V presents the conclusions.

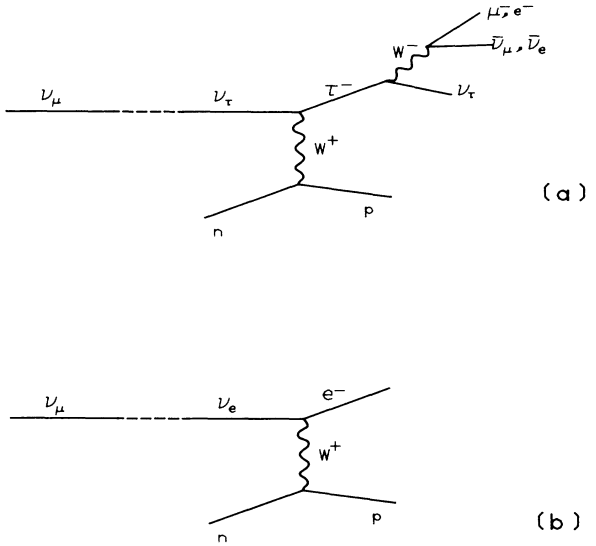

FIG. 1. (a) Symbolic representation of a ν_μ oscillating into a ν_τ with the ν_τ interacting by quasielastically scattering off a target nucleon. The $\tau^\pm$ lepton decays into either $\mu^\pm \nu_\mu \nu_\tau$ or $e^\pm \nu_e \nu_\tau$. (b) Symbolic representation of a ν_μ oscillating into a ν_e with the ν_e interacting by quasielastically scattering off a target nucleon. Note that the outgoing lepton, in this case an electron, indicates the incident neutrino flavor.

II. EXPERIMENTAL APPARATUS

The fine-grained neutrino detector located in Laboratory C at Fermilab was built to study the weak neutral-current interaction by the means of deep-inelastic neutrino-nucleon scattering using the Fermilab narrow-band neutrino beam.[9] The neutral-current study required the neutrino detector to be highly segmented to determine both the energy and angle of the recoil hadronic shower. Because of this highly segmented construction and a flexible trigger design, the apparatus could also detect and measure quasielastic neutrino-nucleon scattering. The fine-grained design therefore made the device suitable for a neutrino oscillation search where the quasielastic channel, with its clean energy constraints in a narrow-band beam, could be exploited. Recoil protons could be observed as low as 300 MeV kinetic energy and electron showers could be distinguished from hadronic showers. The outgoing muon momentum was reconstructed with an iron toroid spectrometer placed behind the calorimeter. Thus both muon-neutrino and electron-neutrino quasielastic scattering could be measured.

A. The calorimeter

The calorimeter[5] is based on 608 polypropylene flash chambers and 37 proportional tube chambers. The device is 18.3 m long and 3.6×3.6 m^2 in cross section. The calorimeter mass is 340 metric tons and has an average density of 1.4 g/cm^3. The neutrino target material consists of plastic extrusions filled with sand and steel shot in alternating layers which makes the detector massive but with a low atomic number. Figure 2 gives an overview of the detector.

The construction of the calorimeter is modular. The flash chambers are used to determine the type of neutrino interaction and to measure the shower energy and angle of the reaction products. The proportional tube

chambers provide the trigger for the flash chambers and furnish an independent measurement of the shower energy. The flash chambers are assembled in units of four in the sequence of *U-X-Y-X*. The *U-X-Y* flash chambers are constructed with their cells at 100-0-80 degrees about the horizontal plane. The proportional tube chambers have wires alternating in the horizontal and vertical directions and are located at intervals of 16 flash chamber planes. These chambers sample the shower in 10 cm lateral segments (approximately a Moliere radius).

The longitudinal shower sampling of the flash chambers is 22% of a radiation length and 3.1% of an absorption length. The proportional tube chambers sample the shower in the longitudinal direction every 3.5 radiation lengths and every 0.49 absorption length. The fine granularity permits electron showers to be separated from hadronic showers with only a few percent hadronic shower contamination for energies up to 50 GeV. The pattern-recognition capabilities allow recoil protons from quasielastic scattering to be detected and the outgoing muon tracks from ν_μ-nucleon quasielastic scattering to be easily reconstructed.

B. The muon spectrometer

The muon spectrometer[5] consists of three 7.31-m- and four 3.66-m-diameter magnetized iron toroids located

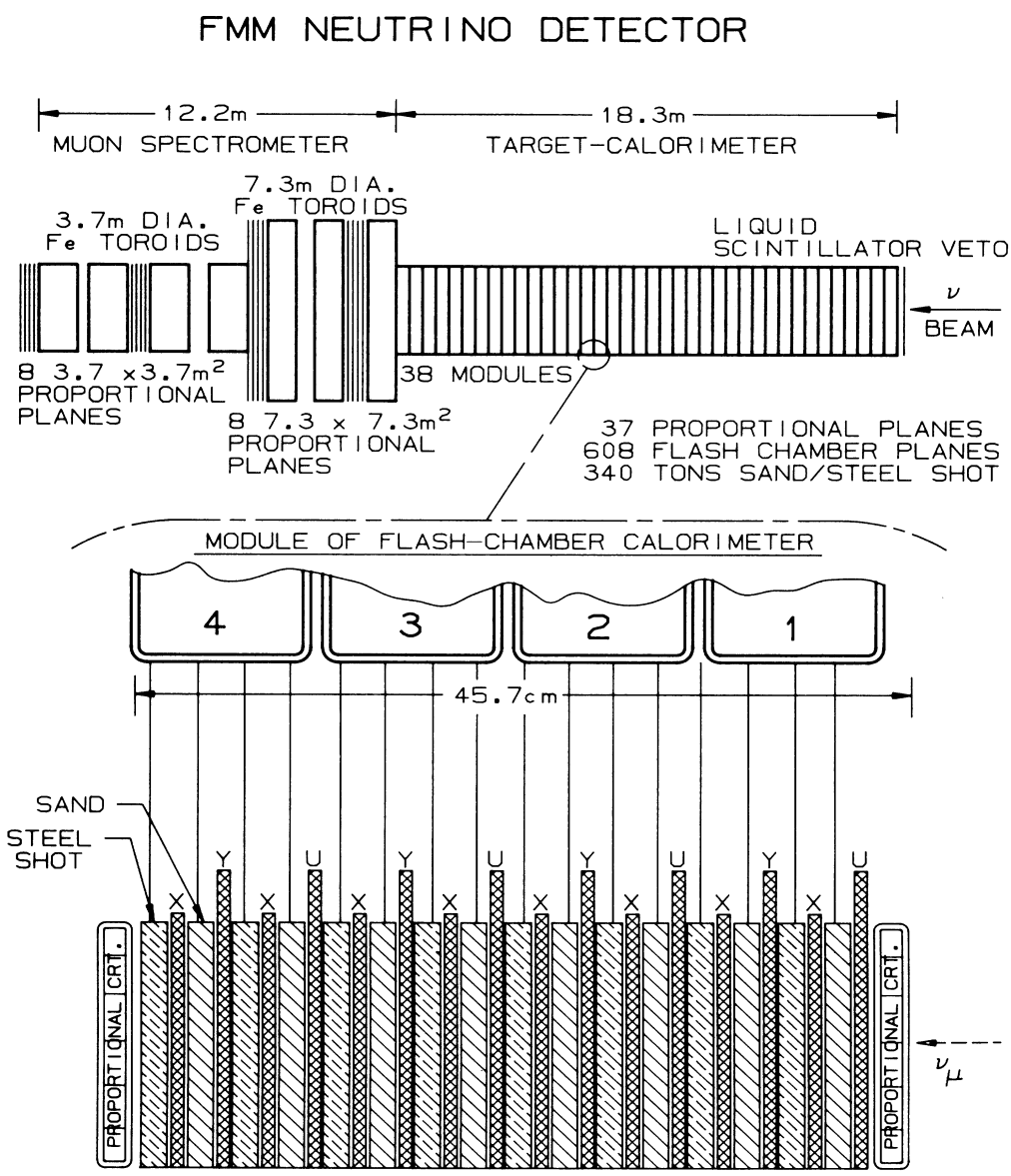

FIG. 2. A schematic drawing of our 340-metric-ton calorimeter is shown. The toroid muon spectrometer located behind the calorimeter is used to analyze the momenta of outgoing muons from the neutrino interaction. Shown below is a detailed schematic of one module of the calorimeter. A module is made from 16 flash chambers layered between plastic extrusions alternately filled with sand and steel shot. Proportional tube chambers placed at intervals of every 16 flash chambers provide the trigger for the flash chambers and furnish an independent measure of the energy deposited in the calorimeter.

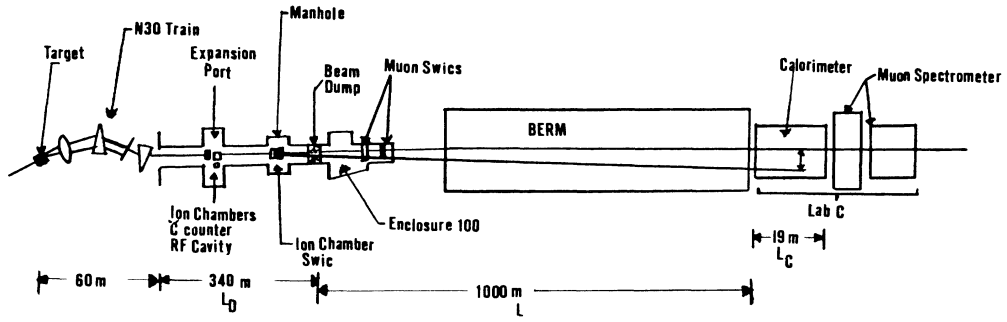

FIG. 3. The layout of the dichromatic neutrino beam at Fermilab. Shown is a schematic outline of the beam transport system which defines the momentum of the secondary pions and kaons of the beam, the secondary beam monitors, and the location of our experiment at Laboratory C. Note that the drawing is not to scale, although the relevant distances are indicated. For simplicity the other neutrino detectors in the beam line have not been shown.

just downstream of the flash-chamber–proportional-tube calorimeter. There are roughly 7 m of magnetized iron in the spectrometer. Four gaps between the toroids are instrumented with proportional chambers which determine the position of the muon track to an rms spatial precision of about 0.73 cm. These chambers are constructed in a double layer with a half-cell offset to resolve the left-right ambiguity. A muon momentum resolution is achieved which is approximately the multiple-scattering limit of the spectrometer $\sigma(p)_\mu/p_\mu \leq 15\%$.

C. The narrow-band beam

The neutrino energy spectrum and the absolute flux are known in the narrow-band beam. The beam is operated by momentum-selecting pions and kaons with a momentum bite of $\sigma(P_0)/P_0 \approx 10\%$ using a magnetic beam transport system.[9] The momentum-selected pions and kaons decay in a 340-m-long evacuated beam pipe producing a neutrino energy spectrum with two distinct energy bands corresponding to the two-meson decays. A schematic diagram of the beam layout is shown in Fig. 3.

The energy of the incident neutrino of the narrow-band beam depended on the mass of the decaying meson and on the angle of the neutrino with respect to the secondary beam direction. From the kinematics of the secondary particle (pion or kaon) decay the energy of the incident neutrino is given by

$$E_\nu \approx (m^2 - m_\mu^2)(m^2/P_0 + P_0\theta_\nu^2) , \quad (2)$$

where m is the pion or kaon rest mass, m_μ is the muon rest mass, P_0 is the pion-kaon central momentum, and θ_ν is the angle of the neutrino with respect to the parent beam direction in the laboratory frame. The angle of the neutrino was estimated from the radius of the event vertex about the centroid of the incident neutrino beam. A typical measured energy-versus-radius correlation is shown in Fig. 4. The data are muon-neutrino quasielastic events taken with the narrow-band beam set to focus 165 GeV/c positive secondaries. The kaon and pion energy bands are apparent.

The narrow-band pion and kaon secondary beam momentum was set at 165, 200, and 250 GeV/c to focus positive secondaries for the neutrino data. The antineutrino data were taken at 165 GeV/c with the beam set to focus negative secondaries.

III. DATA ANALYSIS

In this section we describe the analysis procedure for each of the three reaction chains given above. The

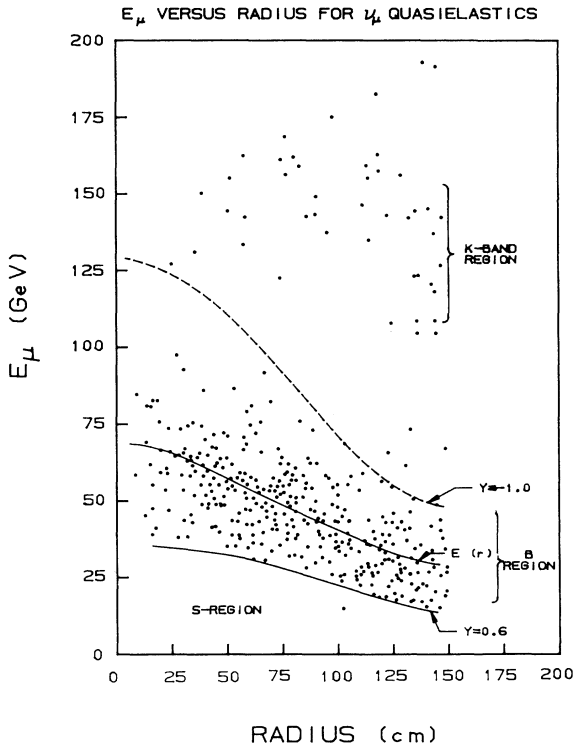

FIG. 4. The energy vs radius correlation of the dichromatic neutrino beam as measured by the outgoing muon energy for muon-neutrino quasielastic events. The data are from the +165-GeV/c beam setting. The $\nu_\mu \rightarrow \nu_\tau$ oscillation domain is indicated by the S region. The region where the ordinary muon-neutrino quasielastic events are confined is indicated by the area B in the figure. Shown are the boundary lines defined in the text by the limits $-1.0 < y_\mu < 0.6$. The predicted average neutrino energy $E_\nu^\pi(r)$ used in the text is indicated by the line $E(r)$.

analysis involved searching for a single muon or electron shower consistent with a ν_τ or a ν_e quasielastic neutrino-nucleon interaction. To select the quasielastic topology we required the hadronic energy of the candidate events to be less than 1 GeV in the flash chamber calorimeter. A further condition was imposed by requiring that there be a clearly identified muon track or electron shower emerging from the primary vertex.

A ν_τ quasielastic event, where $\tau^\pm$ has decayed into either a muon and two neutrinos or an electron and two neutrinos, has a predicted event signature which resembles the ordinary quasielastic scattering of a muon or an electron neutrino. However, the reconstructed energy of the event will be smaller than expected since there will be energy carried away by the undetected neutrinos from the $\tau^\pm$ decay. The missing energy can be calculated by comparing the measured event energy to the incident neutrino energy predicted by the energy-versus-radius correlation of the narrow-band beam. Therefore, by requiring that there be a significant amount of missing energy we can distinguish the $\nu_\mu \rightarrow \nu_\tau$ neutrino-oscillation candidates from the background events. Only leptonic decays of the charged τ lepton were considered since the hadronic decays of the τ lepton have an event topology which is difficult to separate from the abundant muon-neutrino neutral-current events.

A. Case A: $\nu_\mu \rightarrow \nu_\tau$ decay muon channel

In the decay muon channel (case A) we searched for the possibility of a muon neutrino oscillating into a tau neutrino which interacts quasielastically with a target nucleon followed by the produced $\tau^\pm$ lepton decaying into a $\mu^\pm \nu_\mu \nu_\tau$. The branching ratio for this decay mode has been measured[10] to be $(17.6 \pm 0.6)\%$. The signature of the quasielastic ν_τ-nucleon interaction followed by the $\tau^\pm$ decay is a single outgoing muon track with an energy smaller than that expected from quasielastic scattering in the narrow-band beam. The missing energy corresponding to the unobserved neutrinos in the $\tau^\pm$ decay is computed by comparing the outgoing muon energy, which carries essentially all of the event energy for an ordinary muon-neutrino quasielastic interaction,[8] with the expected neutrino energy computed from the energy-versus-radius correlation of the narrow-band neutrino beam.

The quasielastic events satisfied a trigger condition which required the muon to reach the back chambers of the muon spectrometer (roughly 7 m of iron) and a total energy deposition in the calorimeter of less than 10 GeV. The outgoing muon track could deposit up to 5 GeV in the calorimeter. Therefore, only a relatively small fraction of the incident neutrino energy was allowed to be deposited in the hadronic sector. The efficiency of this trigger condition was about 80% for true ν_μ quasielastic events and was measured by calibration beam muons analyzed to simulate the trigger.

The final selection of the neutrino-oscillation candidates required that the outgoing muons have an energy $E_\mu > 10$ GeV. Additional requirements were imposed to ensure that the radius of the event vertex was within 150 cm of the beam central axis and that there be less than 30 flash chamber hit cells excluding the muon track within a 50-cm radius of the event primary vertex. The latter cut corresponds to an upper bound of hadronic energy of about 1 GeV. Figure 5 shows a typical event selected by these criteria.

While we have made stringent cuts on the amount of energy deposited around the primary vertex to select quasielastic events, we have a contamination of "almost quasielastic" events where the low-lying nucleonic resonances have been excited.[11] An additional complication arises from complex target effects (our calorimeter mass is mostly composed of SiO_2 and Fe with a smaller component of Al and hydrocarbons) which lead to final-state interactions of the outgoing recoil nucleon. These effects do not alter our result because of electron-muon-tau universality. According to this assumption, at the high energies of this experiment where lepton mass effects are small, the nucleon resonance excitation by muon neutrinos will be the same as for electron or tau neutrinos. Furthermore, the complex target final-state interactions are assumed to be independent of the incident neutrino species. Since we internally normalize our data these effects will cancel.

As a check that our data are in agreement with our expectations, we compared the reconstructed momentum transfer Q^2 between the outgoing muon and the incident neutrino with our Monte Carlo simulation for antineutrino events in the pion band energy region. The result is shown in Fig. 6 where we see that the agreement between the data and the Monte Carlo simulation is good. The antineutrino data set has been chosen to avoid the background of inverse muon decay ($\nu_\mu e^- \rightarrow \mu^- \nu_e$).

To separate neutrino-oscillation candidates from ordinary background events a cut was made on the missing energy which arises from the undetected neutrinos of the τ lepton decay. Therefore, most of the ν_τ events are expected to be below the pion energy band. We refer to this region as the signal region S in Fig. 4. The pion energy band, referred to as the background region B in the figure, is the domain where most of the ordinary ν_μ qua-

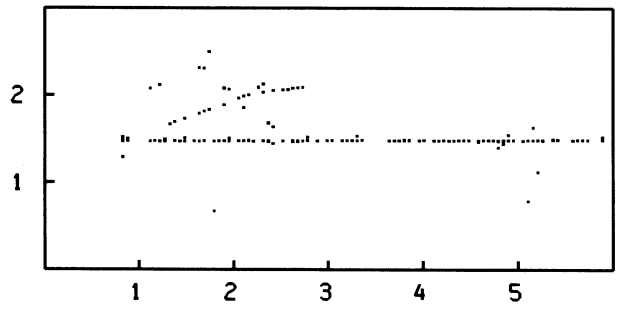

FIG. 5. Computer display of a typical muon-neutrino quasielastic event. Shown are the x-view chambers around the primary vertex. The numbers on the outside of the figure indicate the dimensions of the event in meters. Each dot in the display is a hit cell of a flash chamber. A recoil proton and an outgoing muon track are clearly visible emanating from the primary vertex. The proton recoil kinetic energy is approximately 1 GeV. The track intersecting the recoil proton is believed to be an accidental cosmic ray.

sielastic events are expected. We have avoided searching for neutrino-oscillation candidates in the region between the pion and kaon energy bands. In that region there is a large flux of neutrinos from the three-body decay modes $K_{\mu 3}$ and K_{e3} which makes the computation of the missing event energy critically dependent on the knowledge of the neutrino flux shape and composition.

The quantitative separation of the $\nu_\mu \rightarrow \nu_\tau$ oscillation signal region S from the background region B is accomplished by selecting events using the scaled energy variable:

$$y_\mu = [\bar{E}_\nu(r) - E_\mu]/\bar{E}_\nu(r) , \quad (3)$$

where $\bar{E}_\nu(r)$ is the predicted average neutrino energy at a given radius arising from pion decay and E_μ is the measured muon energy. Note that positive values of y_μ correspond to missing event energy. The y_μ distributions of the data at the four narrow-band beam settings are compared with the corresponding Monte Carlo simulations of ordinary muon-neutrino quasielastic scattering in Fig. 7. The signal region S was defined by the cut $y_\mu > 0.6$ which optimized the sensitivity to $\nu_\mu \rightarrow \nu_\tau$ oscillations while minimizing the number of true muon-neutrino quasielastic events. The background region was determined by the cuts $-1.0 < y_\mu < 0.6$. These

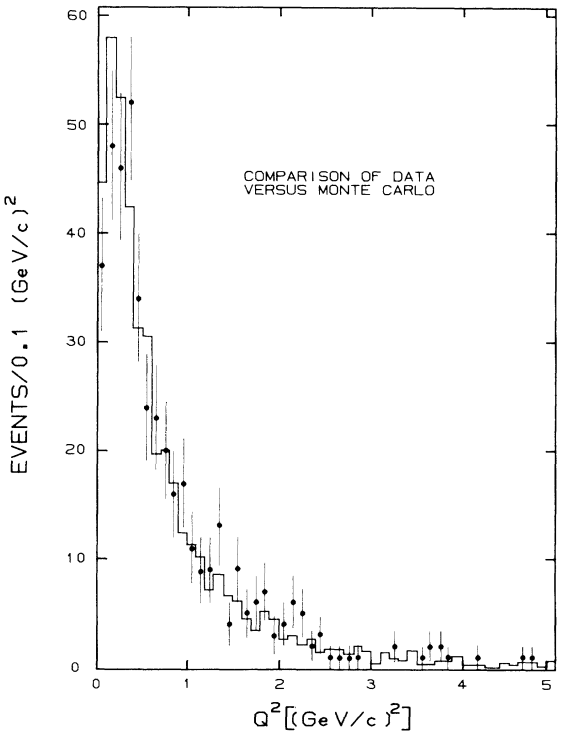

FIG. 6. The Q^2 distribution of muon-neutrino quasielastic scattering data is compared to the Monte Carlo simulation. The data are from the antineutrino beam setting to avoid the inverse muon decay background. The quasielastic events have been selected to be in the oscillation background region B defined in the text. The data are indicated by the points with error bars and the Monte Carlo simulation is denoted by the histogram.

definitions were chosen from a study of the Monte Carlo simulation which required the signal region to contain a factor of 100 less ν_μ quasielastic events than the background region. In the signal region the overall efficiency for ν_τ oscillation events was 15 times higher than the efficiency for ordinary ν_μ quasielastic events.

Table I summarizes the number of observed events (N^B) found in the background region B, the number of events (N^S) in the signal region S, and the calculated efficiencies $\epsilon_\mu^B, \epsilon_\mu^S$ for detecting a ν_μ quasielastic event in the two kinematic regions, respectively. The efficiencies for detecting a ν_τ quasielastic event with the decay mode $\tau^\pm \rightarrow \mu^\pm \nu_\mu \nu_\tau$ in these two regions are given by ϵ_τ^B and ϵ_τ^S. These efficiencies were determined by a Monte Carlo simulation which took into account the acceptance, momentum resolution, and the narrow-band beam characteristics. The muon trigger efficiency was not included in the analysis of the decay muon channel since it cancels in our determination of the oscillation limit.

There were three major backgrounds which contaminate the ν_τ quasielastic candidates. These backgrounds were either included in the Monte Carlo simulation of the experiment or were explicitly subtracted.

(1) The first background was due to muon neutrinos which originate from π or K decays before the momentum selection of the narrow-band beam. By closing the collimator in the secondary pion/kaon beam while taking data, the absolute normalization of this background was fixed. The spectrum shape was computed by a Monte Carlo simulation.[12] The Monte Carlo simulation was compared with the data and, within statistics, the predicted closed collimator background was found to be consistent with the observed spectrum. Using the normalized Monte Carlo simulation, the ratio of the closed collimator background to the standard muon-neutrino flux was 0.4% for the antineutrino setting and 0.6% for the pion band neutrino beam settings.

(2) The second background was due to muon neutrinos which originated from the three-body decay mode $K_{\mu 3}$. The kinematics of the three-body decay can give rise to neutrinos with an energy less than the pion-band energy. Quasielastic events induced by these muon neutrinos will therefore have an apparent missing energy. The magnitude of the background was estimated from the Monte Carlo beam simulation to be 0.2% of the pion-band muon-neutrino flux for the antineutrino setting and 0.6% for the neutrino beam settings.

(3) The third background consisted of events from the inverse muon decay reaction ($\nu_\mu e^- \rightarrow \mu^- \nu_e$) which contributed a signal for incident neutrinos but not for incident antineutrinos by additive lepton number conservation. The detection efficiencies for this process are denoted by ϵ_I^S and ϵ_I^B in Table I. In a separate analysis[13] the observed number of events from this process corrected for detection efficiency was $N_I = 23 \pm 8$ events.

To set limits on the neutrino oscillation mode of case A we define the ratio R_μ^τ to be the number of events of $\nu_\tau n \rightarrow \tau^- p$ followed by the decay $\tau^- \rightarrow \mu^- \nu_\tau \nu_\mu$ (likewise for the corresponding antineutrino case) over the number of ordinary muon-neutrino quasielastic events, N_μ.

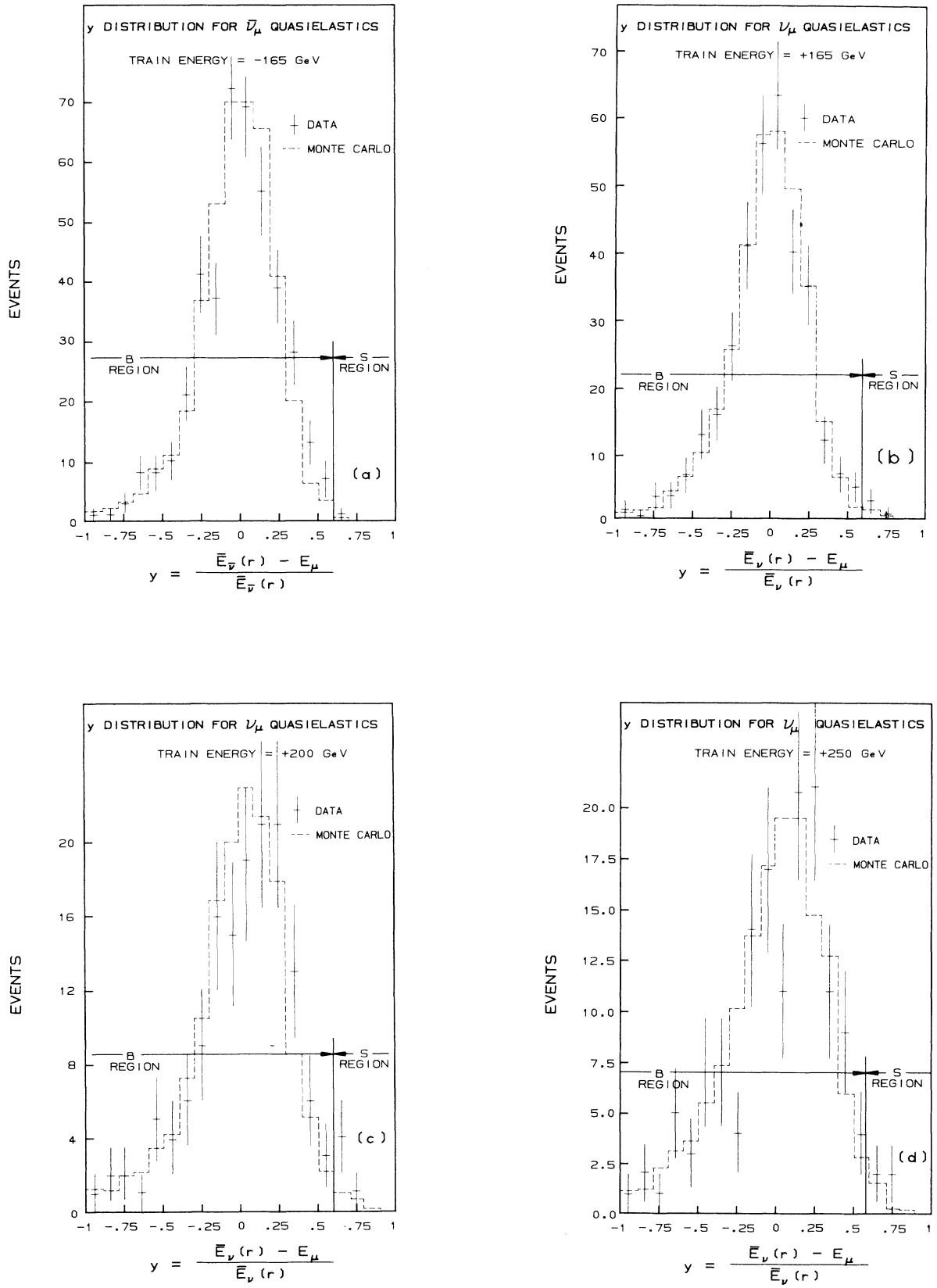

FIG. 7. The y_μ distribution for quasielastic events vs the Monte Carlo simulation. The signal region S and the background region B as defined in the text are shown. (a) -165-GeV/c dichromatic train setting. (b) $+165$-GeV/c dichromatic train setting. (c) $+200$-GeV/c dichromatic train setting. (d) $+250$-GeV/c dichromatic train setting.

TABLE I. Summary of the muon channel (case A). The details of the calculation of the limits of a muon-neutrino to oscillate into a τ neutrino where the τ lepton decays into a muon and two neutrinos are given. The column marked "Mode" denotes the neutrino-oscillation mode. The background region B is the π-band region defined by the $-1.0<y_\mu<0.6$ cut. The signal region S is defined by the cut $y_\mu>0.6$. N^B is the number of events found in the B region. ϵ_μ^B, ϵ_τ^B, $\epsilon_I{}^B$ are the efficiencies defined in the text for the B region. N^S is the number of events found in the S region and ϵ_μ^S, ϵ_τ^S, ϵ_I^S are the corresponding detection efficiencies. $N_I{}^B$ and $N_I{}^S$ are the observed number of inverse muon decay events in the two regions, and are given by $\epsilon_I{}^B N_I$ and $\epsilon_I{}^S N_I$, respectively. Note that $\epsilon_I{}^B$ and $\epsilon_I{}^S$ for antineutrinos are identically zero since the inverse muon decay reaction is forbidden by additive lepton number conservation. The upper limits are given by the columns R_μ^τ and $R_{\mu\,90\%}^\tau$, where the former is the ratio of the number of ν_τ quasielastic events with the $\tau^\pm\to\mu^\pm\nu_\tau\nu_\mu$ decay to the number of ν_μ quasielastic events and the latter is the 90%-confidence-level upper limit of R_μ^τ.

	B region ($-1.0<y_\mu<0.6$)					S region ($y_\mu>0.6$)						
Mode	N^B	ϵ_μ^B	ϵ_τ^B	$\epsilon_I{}^B$	$N_I{}^B$	N^S	ϵ_μ^S	ϵ_τ^S	$\epsilon_I{}^S$	$N_I{}^S$	R_μ^τ	$R_{\mu\,90\%}^\tau$
$\nu_\mu\to\nu_\tau$	614	0.756	0.260	0.64	15	12	0.007	0.105	0.130	3	0.04	0.11
$\bar{\nu}_\mu\to\bar{\nu}_\tau$	405	0.774	0.266	0.0	0	1	0.006	0.089	0.0	0	0.0	0.051

The observed total numbers of events N^S and N^B detected in the two regions S and B are expressed by adding the number of ν_τ quasielastic events given by $N_\mu R_\mu^\tau \epsilon_\tau^{S,B}$, the number of ordinary ν_μ quasielastic events which is denoted by $N_\mu \epsilon_\mu^{S,B}$, and the number of inverse muon decay events ($\nu_\mu e^-\to\mu^-\nu_e$) $N_I \epsilon_I^{S,B}$. Thus,

$$N^S = N_\mu(R_\mu^\tau \epsilon_\tau^S + \epsilon_\mu^S) + N_I \epsilon_I^S \ , \tag{4a}$$

$$N^B = N_\mu(R_\mu^\tau \epsilon_\tau^B + \epsilon_\mu^B) + N_I \epsilon_I^B \ . \tag{4b}$$

Equations (4a) and (4b) are then solved for the ratio R_μ^τ defined above and the number of quasielastic events N_μ corrected for the detection efficiencies defined above. The result is

$$R_\mu^\tau = (\epsilon_\mu^S - \eta\epsilon_\mu^B)/(\eta\epsilon_\tau^B - \epsilon_\tau^S) \ , \tag{5}$$

where $\eta = (N^S - N_I\epsilon_I^S)/(N^B - N_I\epsilon_I^B)$ and the corrected number of muon-neutrino quasielastic events is

$$N_\mu = (N^S - N_I\epsilon_I^S)/(R_\mu^\tau \epsilon_\tau^S + \epsilon_\mu^S) \ . \tag{6}$$

The results for R_μ^τ and its 90%-confidence upper limit $R_{\mu\,90\%}^\tau$ are given in the last two columns of Table I. We see that $R_\mu^\tau = 0.04$ (0.0) and $R_{\mu\,90\%}^\tau = 0.11$ (0.051) for ν_μ ($\bar{\nu}_\mu$).

B. Case B: $\nu_\mu\to\nu_\tau$ decay electron channel

In this channel we searched for the possibility of a muon neutrino to oscillate into a τ neutrino which interacts quasielastically with the target nucleon followed by the τ lepton decaying into an electron and two neutrinos ($\tau^\pm\to e^\pm\nu_e\nu_\mu$). The signature for this process is an electromagnetic shower which satisfies the energy deposition trigger in the calorimeter ($E_{\text{calorimeter}} > 10$ GeV) but with an energy less than that expected from the narrow-band beam pion band. An additional criterion which diminished the deep-inelastic muon-neutrino neutral-current background was imposed by requiring the transverse momentum about the incident neutrino axis be small ($P_\perp < 2$ GeV/c) since almost all quasielastic events are at small Q^2. A typical $\nu_e N\to e^- P$ quasielastic candidate event selected by these criteria is shown in Fig. 8.

There is a significant neutral-current background in case B arising from ν_μ-nucleon deep-inelastic scattering. These events can have dense hadronic showers which therefore imitate the expected event characteristics. Some reduction of the neutral-current background is achieved by making energy and transverse-momentum cuts on the recoil electromagnetic shower. But these cuts are not sufficient to entirely eliminate this large background. Therefore, a software filter was designed to distinguish electromagnetic showers from hadronic showers. This filter utilized the characteristics that electromagnetic showers are small in their transverse dimension, dense, and are not surrounded by visible tracks in the flash chamber calorimeter. By using calibration electron and hadron showers, we determined that the filter was >99% efficient for electron showers above 10 GeV and had a hadronic shower rejection efficiency which ranged from 96% at 10 GeV to 99% at 75 GeV.

To estimate the hadronic background from muon-neutrino neutral-current deep-inelastic scattering, we as-

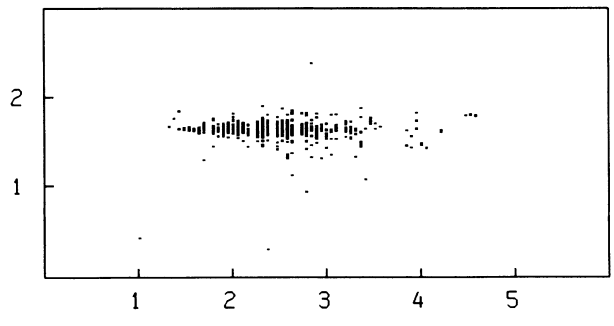

FIG. 8. A typical electron-neutrino quasielastic scattering event. For simplicity only the x-flash chamber view is shown. Each dot in the figure is a 5×5-mm^2 hit cell. The recoil shower is identified as an electromagnetic shower because of the dense energy deposition with no visible tracks within the shower body. A small recoil proton stub coming from the primary vertex is visible which has an estimated kinetic energy of 300 MeV. The size of the event is indicated by the grid on the border of the diagram marked in meters.

TABLE II. Summary of the electron decay channel (case B). A summary of the muon-neutrino to τ-neutrino oscillation case where the τ decays into an electron and two neutrinos is shown. The column marked "Mode" denotes the neutrino-flavor oscillation mode. C and N are the number of charged-current and neutral-current deep-inelastic-scattering events used to determine the dense neutral-current background. The heading marked "Before filter" shows the number of events before the electromagnetic filter was applied but after the y_e cut was made. The ratio $N/C = r_\mu$ is used in Eqs. (8) and (9). The column "After all cuts" denotes the number of events after the filter and all cuts were applied. The number of coherent π^0 background events satisfying the cuts is given by n_{π^0}. The number of quasielastic signature events corrected for the software and trigger efficiency is given by n_μ. The efficiency to detect a ν_τ quasielastic event is ϵ_τ^e. R_e^τ is the ratio of ν_τ to ν_μ quasielastic events and $R_{e\,90\%}^\tau$ is the 90%-confidence limit of R_e^τ.

	Before filter		After all cuts						
Mode	C	N	$C_{\rm em}$	$N_{\rm em}$	n_{π^0}	n_μ	ϵ_τ^e	R_e^τ	$R_{e\,90\%}^\tau$
$\nu_\mu \to \nu_\tau$	9947	3006	118	47	4.2	795	0.65	0.0112	0.030
$\bar{\nu}_\mu \to \bar{\nu}_\tau$	3295	1283	63	24	3.1	482	0.63	−0.0134	0.012

sumed that the fraction of neutral-current deep-inelastic-scattering events which has a large electromagnetic component is the same fraction as in charged-current deep-inelastic scattering. The hadronic background was therefore determined by applying the filter to all charged-current deep-inelastic-scattering events. In this study charged-current events were selected with the same cuts as were applied to the oscillation candidates. These cuts required that the events have a radius about the central neutrino beam axis of less than 120 cm for good lateral shower containment and a shower energy $E_S > 10$ GeV. An additional cut was made in the scaled energy variable defined by

$$y_e = [\bar{E}_\nu(r) - E_S]/\bar{E}_\nu(r) , \tag{7}$$

requiring that $y_e > 0.2$, where $\bar{E}_\nu(r)$ is the average incident energy from the pion band at a radius r given by the energy-versus-radius correlation of the narrow-band neutrino beam. The y_e cut demanded that there be missing energy consistent with $\nu_\mu \to \nu_\tau$ oscillation followed by the $\tau^\pm$ decay into $e^\pm \nu_e \nu_\tau$. An additional requirement was imposed that the transverse momentum of the shower ($P_\perp$) with respect to the neutrino direction be less than 2 GeV/c to suppress deep-inelastic neutrino-nucleon scattering.

Other backgrounds include neutral-current coherent π^0 production from nuclei ($\nu_\mu N \to \nu_\mu N \pi^0$) (Ref. 14), coherent γ production from nuclei ($\nu_\mu N \to \nu_\mu N \gamma$) (Ref. 15), and resonant π^0 production.[11] The coherent π^0 process contributes a significant background to case B since it has a sizable cross section compared to the quasielastic cross section and a (1-y) dependence [$y = E_{\pi^0}/E_\nu^\pi(r)$] which allows the π^0 energy to be in the signal energy region below the pion neutrino band. Furthermore, the π^0 electromagnetic showers are indistinguishable from electron showers in our calorimeter. The coherent single γ process is expected to have a small cross section (about 0.5% of the coherent π^0 cross section at 50 GeV) and therefore it does not contribute much background. The resonant π^0 production is expected to produce electromagnetic showers at quite low energies (< 1 GeV) since the π^0 from this process comes from N^* decay which is produced at low Q^2 by form-factor effects. Therefore, this background will be strongly suppressed since it will produce electromagnetic showers which are largely below the threshold of the energy-deposition trigger.

We have considered two other backgrounds: (1) electron neutrinos (from K_{e3} decay) that scatter quasielastically off nucleons ($\nu_e N$) and (2) muon neutrinos which elastically scatter off electrons in the target ($\nu_\mu e$). Both of these reactions give rise to electron showers which have the characteristics of the oscillation candidates for which we are searching.

The oscillation limit is computed by subtracting the backgrounds from the neutral-current events which have identified electromagnetic showers ($N_{\rm em}$ data sample). The largest background arises from the neutral-current deep-inelastic-scattering events as was discussed above. This background is followed in significance by coherent π^0 production by the neutral current. We estimate that the coherent π^0 process contributes 4.2 background events for incident neutrinos and 3.1 background events for incident antineutrinos. By a Monte Carlo simulation the ($\nu_e N$) and ($\nu_\mu e$) backgrounds[16,17] both contribute 0.68 events for incident neutrinos, and 0.14 and 0.31 for antineutrinos, respectively. We have neglected the coherent γ process and resonant π^0 production.

The first two columns in Table II show the number of charged-current (C) and neutral-current (N) events found in the sample before the electromagnetic shower filter cuts. In the third and fourth columns the electron filter cut and the transverse momentum cut have been imposed. We denote the resulting numbers of events after these cuts by $C_{\rm em}$ and $N_{\rm em}$, respectively. The neutral-current deep-inelastic background was estimated by determining the number of charged-current events which satisfy the electron filter $C_{\rm em}$ corrected for the ratio r_μ of neutral-current to charged-current events.

As in the muon channel case, we define R_e^τ as the ratio of the number of events n_τ of the type $\nu_\tau N \to \tau^- P$ with the τ^- subsequently decaying into $e^- \bar{\nu}_e \nu_\tau$ over the number of events n_μ of the type $\nu_\mu N \to \mu^- P$. The limit for incident antineutrinos was treated in the same manner. The value of $R_e^\tau = n_\tau/n_\mu$ can be calculated by using the

TABLE III. Summary of the electron-neutrino channel (case C). The upper limits on the muon-neutrino to oscillate into an electron-neutrino are listed. The column marked "Mode" denotes the oscillation channel considered. C and N are the number of charged-current and neutral-current deep-inelastic-scattering events, respectively. The "Before filter" and "After filter" columns pertain to before and after the electromagnetic filter cut. The coherent π^0 background is given by n_{π^0}. The number of muon-neutrino quasielastic events used for the rate normalization is given by n_μ. ϵ_e^e is the efficiency to detect a ν_e quasielastic event, R_e^e is the ratio of ν_e to ν_μ quasielastic events and $R_{e\,90\%}^e$ is the 90%-confidence upper limit of R_e^e.

	Before filter		After filter						
Mode	C	N	$C_{\rm em}$	$N_{\rm em}$	n_{π^0}	n_μ	ϵ_e^e	R_e^e	$R_{e\,90\%}^e$
$\nu_\mu \rightarrow \nu_e$	9947	3006	6	2	0.59	795	0.60	−0.0096	0.007
$\bar{\nu}_\mu \rightarrow \bar{\nu}_e$	3295	1283	1	3	0.27	482	0.60	0.0055	0.020

relation which expresses the number of observed ν_τ candidates $n_\tau \epsilon_\tau^e$ in terms of the number of observed electromagnetic events corrected for the four backgrounds discussed above. ϵ_τ^e is the detection efficiency calculated by Monte Carlo methods for finding an electron from the decay of the τ in a quasielastic reaction. This relation is

$$R_e^\tau = (N_{\rm em} - r_\mu C_{\rm em} - n_{\pi^0} - n_{\nu_e N} - n_{\nu_\mu e})/n_\mu \epsilon_\tau^e , \quad (8)$$

where n_μ is the number of ν_μ quasielastic events found in the previous muon channel analysis (N_μ) corrected for the trigger efficiency (80%) and the less restrictive radius cut ($r < 120$ cm) and r_μ is the ratio of the neutral-current to charged-current events found from our deep-inelastic-scattering data sample before applying the filter and $P_\perp$ cuts, but after the correction for the K_{e3} background. n_{π^0} is the calculated number of coherent π^0 events accepted by the cuts, $n_{\nu_e N}$ is the calculated number of background ν_e quasielastic signature events, $n_{\nu_\mu e}$ is the estimated number of background ν_μ-electron elastic events. Referring to the last two columns of Table II we find that the ratio R_e^τ was determined to be 0.0112 and −0.0134 for the neutrino and antineutrino cases, respectively. The corresponding 90%-confidence upper limits are 0.030 and 0.012.

C. Case C: $\nu_\mu \rightarrow \nu_e$ electron-neutrino oscillation channel

In the electron-neutrino oscillation channel, case C, we searched for the possibility of a muon neutrino (ν_μ) oscillating into an electron neutrino (ν_e), where the electron neutrino interacts quasielastically with a target nucleon. The signature for this reaction sequence is a single electromagnetic shower in the calorimeter with no significant missing energy and a small transverse momentum with respect to the incident neutrino beam axis.

Electromagnetic showers were selected from the deep-inelastic sample ($N+C$ events) with the aid of the previously defined filter. The oscillation data sample was formed by the events which passed the electromagnetic shower filter with the additional requirements that $-0.2 < y_e < 0.2$, where y_e is defined by Eq. (7) above, and the transverse momentum $P_\perp$ of the electron shower about the incident neutrino direction be less than 1.5 GeV/c. The number of events which passed these cuts is given in Table III.

The $\nu_\mu \rightarrow \nu_e$ oscillation limit is computed in the same manner as in case B described above. Defining R_e^e as the ratio of the number of electron-neutrino quasielastic scattering candidate events to the number of events from the process $\nu_\mu N \rightarrow \mu^- P$ (and the corresponding antineutrino reactions), we have the relation

$$R_e^e = (N_{\rm em} - r_\mu C_{\rm em} - n_{\pi^0} - n_{\nu_e N} - n_{\nu_\mu e})/n_\mu \epsilon_e^e , \quad (9)$$

where all of the quantities in this equation are defined in the same manner as in case B above. Note that ϵ_e^e is the efficiency for detecting an electron-neutrino quasielastic event with the $P_\perp < 1.5$ GeV/c. In this case the number $n_{\nu_\mu e}$ of background events from the muon neutrino-electron elastic scattering is 0.20 and 0.12 for the incident neutrino and antineutrino beams, respectively. The number $n_{\nu_e N}$ of electron neutrino quasielastic scattering events is 3.97 for incident neutrinos and 0.62 for incident antineutrinos. The coherent π^0 process contributes 0.59 and 0.27 events for neutrinos and antineutrinos, respectively. Referring to Table III, the upper limits are $R_e^e = -0.0096$ (0.0055) and the 90%-confidence-level upper limits are $R_{e\,90\%}^e = 0.007$ (0.02) for the neutrino (antineutrino) cases.

IV. DETERMINATION OF THE OSCILLATION UPPER LIMITS

By interpreting the upper limits given in Tables I–III in terms of upper limits from neutrino oscillations in the channels discussed above, we obtain a limit on the oscillation probability $P(\nu_\mu \rightarrow \nu_\tau)$ given by Eq. (1) through the relation

$$R^\tau = \frac{\int dQ^2 dE_\nu \phi(E_\nu) P(\nu_\mu \rightarrow \nu_\tau) d^2\sigma^\tau / dQ^2 dE_\nu}{\int dQ^2 dE_\nu \phi(E_\nu) d^2\sigma^\mu / dQ^2 dE_\nu} \Gamma , \quad (10)$$

where $\phi(E_\nu)$ is the incident neutrino flux, E_ν is the incoming neutrino energy in GeV, and $d^2\sigma^{\tau,\mu}/dQ^2 dE_\nu$ is the quasielastic differential cross section for ν_τ and ν_μ, respectively. Γ is the branching ratio for the leptonic decays of the τ lepton under consideration. Equation (10) can be solved numerically in terms of the neutrino flavor mixing angle θ and the mass-squared difference Δm^2 for the oscillating pair of neutrino flavors.

As is evident from Tables I and II the best limit on the $\nu_\mu \to \nu_\tau$ oscillation hypothesis comes from the $\tau \to e\nu_\tau\nu_e$ branching fraction given in Table II. Figure 9 shows the result of evaluating Eq. (10) for this τ-decay electron channel (case B). In the limit of maximal mixing, the upper limit at the 90% confidence level for $\nu_\mu \to \nu_\tau$ is $\Delta m^2 < 10.2$ eV^2 and for the antineutrino case $\bar{\nu}_\mu \to \bar{\nu}_\tau$, $\Delta m^2 < 6.5$ eV^2. In the limit where Δm^2 becomes large we find that the mixing angle θ has to satisfy the following limits: for $\nu_\mu \to \nu_\tau$, $\sin^2 2\theta < 0.34$; for $\bar{\nu}_\mu \to \bar{\nu}_\tau$, $\sin^2 2\theta < 0.15$. The muon-decay channel limits are less restrictive: for $\nu_\mu \to \nu_\tau$ in the case of maximal mixing, we found $\Delta m^2 < 26.6$ eV^2; for $\bar{\nu}_\mu \to \bar{\nu}_\tau$, $\Delta m^2 < 13.4$ eV^2. There is essentially no restriction from the muon-decay channel on $\sin^2 2\theta$ in the large-Δm^2 limit.

For case C, where we searched for the possibility of $\nu_\mu \to \nu_e$ and $\bar{\nu}_\mu \to \bar{\nu}_e$ oscillations, we interpret the results from Table III through Eq. (10) to obtain the following results: for $\nu_\mu \to \nu_e$ oscillation $\Delta m^2 < 1.8$ eV^2 and for $\bar{\nu}_\mu \to \bar{\nu}_e$, $\Delta m^2 < 3.1$ eV^2 for maximal flavor mixing. Our result for the excluded Δm^2 vs $\sin^2 2\theta$ region is shown in Fig. 10. In the large-Δm^2 region we find for $\nu_\mu \to \nu_e$ $\sin^2 2\theta < 0.015$; for $\bar{\nu}_\mu \to \bar{\nu}_e$, $\sin^2 2\theta < 0.04$. We have set $\Gamma = 1$ in Eq. (10) since there are no branching ratios involved.

V. CONCLUSION

We have set limits on the probabilities $P(\nu_\mu \to \nu_{\tau,e})$ for a muon neutrino to oscillate into either a τ neutrino or an electron neutrino. The experimental sensitivity to the neutrino oscillations was optimized by selecting quasielastic neutrino-nucleon scattering in a narrow-band neutrino beam. This has the advantage of emphasizing the lepton sector which is unique to each incident neutrino flavor. Furthermore, the energy constraints of the narrow-band neutrino beam enabled simple energy cuts to be applied to the data to isolate the oscillation candidates. This technique allows for a straightforward analysis. No evidence for neutrino oscillations was found.

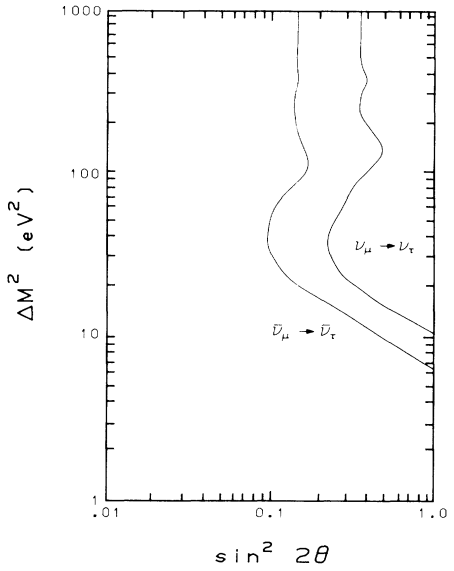

FIG. 9. The Δm^2 vs $\sin^2 2\theta$ correlation upper limits at the 90%-confidence level for $\nu_\mu \to \nu_\tau$ and $\bar{\nu}_\mu \to \bar{\nu}_\tau$ oscillations are shown. The excluded region is the area to the upper right of the curves. The neutrino case $\nu_\mu \to \nu_\tau$ is given by the upper curve and the upper limit for the antineutrino case $\bar{\nu}_\mu \to \bar{\nu}_\tau$ is given by the lower curve. The limits were calculated from case B only.

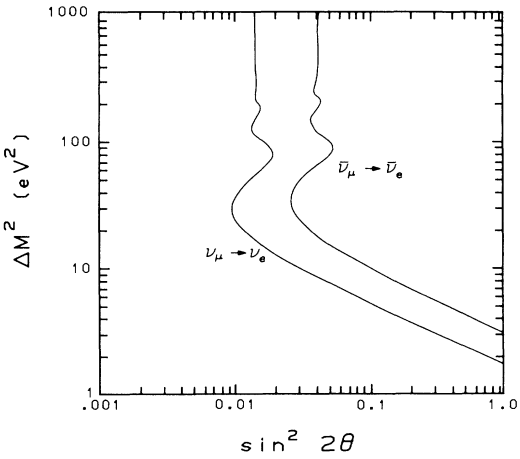

FIG. 10. The Δm^2 vs $\sin^2 2\theta$ correlation for the upper limit at the 90% confidence level for $\nu_\mu \to \nu_e$ oscillations case C of this experiment. The lower curve is for the neutrino case $\nu_\mu \to \nu_e$ and the upper curve is for the antineutrino case $\bar{\nu}_\mu \to \bar{\nu}_e$. The excluded region is shown in the upper right part of the graph.

The best limit on $\nu_\mu \to \nu_\tau$ oscillations from an exclusive-type experiment is $\Delta m^2 < 0.9$ eV^2 (90% confidence limit) from E531 at Fermilab.[18,19] For the antineutrino case, $\bar{\nu}_\mu \to \bar{\nu}_\tau$, the best limit is from the ITEP-Fermilab-Michigan experiment[20] which finds $\Delta m^2 < 2.2$ eV^2. The 90%-confidence-level upper limit for the $\nu_\mu \to \nu_e$ oscillation channel in an exclusive-type experiment has been found to be $\Delta m^2 < 0.09$ eV^2 from a BEBC experiment.[21] In the antineutrino case $\bar{\nu}_\mu \to \bar{\nu}_e$ a limit has been set of $\Delta m^2 < 1.0$ eV^2 from the Gargamelle–Proton Synchrotron Collaboration.[22] A recent BNL experiment of Ahrens *et al.*,[23] finds the limit $\Delta m^2 < 0.43$ eV^2 for maximal mixing. Our limits in both the τ and the electron oscillation channels are somewhat less restrictive but our technique is quite different from that of the other experiments.

The issues of neutrino-flavor nonconservation and neutrino mass are still open. Very sensitive searches for neutrino-flavor nonconservation have been performed by the means of neutrino oscillations. To date, no convincing evidence has been given for the existence of the effect.[24] Further experimentation with a much greater sensitivity is needed to make a significant contribution to this subject.[25]

ACKNOWLEDGMENTS

We would like to thank the National Science Foundation and the U.S. Department of Energy for funding this work. The experiment would not be possible without the fine technical support of Fermilab, MIT, and MSU.

[a]Present address: Fermi National Accelerator Laboratory, Batavia, IL 60510.
[b]Present address: Hughes Aircraft Co., Los Angeles, CA 90009.
[c]Present address: Argonne National Laboratory, Argonne, IL 60439.
[d]Present address: Union College, Schenectady, New York 12308.
[e]Present address: Bell Telephone Laboratory, Naperville, IL.
[f]Present address: Institute of Physics, Warsaw University, Warsaw, Poland.
[g]Present address: Michigan State University, E. Lansing, MI 48824.
[h]Present address: Boston University, Boston, MA 02215.
[i]Permanent address: Illinois Institute of Technology, Chicago, IL 60616.
[j]Present address: University of Florida, Gainesville, FL 32601.
[k]Present address: University of Illinois at Chicago, Box 4348, Chicago, IL 60680.
[l]Permanent address: CEN Saclay, B.P. No. 2, F-91191 Gif-sur-Yvette, France.

[1]The case for three simultaneously oscillating neutrino flavors has been reviewed by H. Blumer and K. Kleinknecht, Phys. Lett. **161B**, 407 (1985), and references therein. For reasons of simplicity we consider only two simultaneously oscillating neutrino flavors.
[2]B. Kayser, Phys. Rev. D **24**, 110 (1981).
[3]B. Pontecorvo, Zh. Eksp. Teor. Fiz. **33**, 549 (1958) [Sov. Phys. JETP **6**, 429 (1958)]; **53**, 1717 (1967) [**26**, 984 (1968)]; S. M. Bilenky and B. Pontecorvo, Phys. Rep. **41**, 225 (1978).
[4]Preliminary versions of this work were presented in Juan Bofill Abadias, Ph.D. thesis, Massachusetts Institute of Technology, 1984; D. Bogert *et al.*, in *Beyond The Standard Model,* proceedings of the XVIII Rencontre de Moriond, La Plagne, France, 1983, edited by J. Tran Thanh Van (Editions Frontiéres, Gif-sur-Yvette, 1983), Vol. 2, p. 53.
[5]D. Bogert *et al.*, IEEE Trans. Nucl. Sci. **NS-29**, 363 (1982); J. Bofill *et al.*, *ibid.* **NS-29**, 400 (1982); F. E. Taylor *et al.*, *ibid.* **NS-27**, 30 (1980).
[6]D. Bogert *et al.*, Phys. Rev. Lett. **55**, 574 (1985).
[7]D. Bogert *et al.*, Phys. Rev. Lett. **55**, 1969 (1985).
[8]C. H. Llewellyn Smith, Phys. Rep. **3**, 5 (1972); L. M. Sehgal, Lectures at Argonne National Laboratory, 1975, Report No. ANL-HEP-PR 75-45 (unpublished).
[9]D. A. Edwards and F. Sciulli, Fermilab Report No. TM-660, 1976 (unpublished).
[10]The $\tau^{\pm}$ lifetime and branching ratios were taken from the Particle Data Group, M. Aguilar-Benitez *et al.*, Phys. Lett. **170B**, 1 (1986).
[11]D. Rein and L. M. Sehgal, Ann. Phys. (N.Y.) **133**, 79 (1981).
[12]T. F. Eldridge, Ph.D. thesis, Massachusetts Institute of Technology.
[13]R. A. Magahiz, Ph.D. thesis, Massachusetts Institute of Technology.
[14]D. Rein and L. M. Sehgal, Nucl. Phys. **B223**, 29 (1983); K. Lackner, *ibid.* **B153**, 526 (1979); for experimental data, see H. Faissner *et al.*, Phys. Lett. **125B**, 230 (1983); E. Isiksal, D. Rein, and J. G. Morfin, Phys. Rev. Lett. **52**, 1096 (1984); F. Bergsma *et al.*, Phys. Lett. **157B**, 469 (1985); C. Baltay *et al.*, Phys. Rev. Lett. **57**, 2629 (1986).
[15]D. Rein and L. M. Sehgal, Phys. Lett. **104B**, 394 (1981).
[16]The cross section for electron-neutrino quasielastic scattering was taken from Ref. 8 assuming e-μ universality.
[17]Recent experimental determinations of the muon neutrino-electron elastic scattering are the following. CHARM Collaboration, M. Jonker *et al.*, Phys. Lett. **117B**, 272 (1982); F. Bergsma *et al.*, *ibid.* **122B**, 465 (1983); L. A. Ahrens *et al.*, Phys. Rev. Lett. **54**, 18 (1985). In an engineering run we have observed the muon-neutrino electron elastic scattering process. See: D. Bogert *et al.*, in *Quarks, Leptons, and Supersymmetry,* proceedings of the XVII Rencontre de Moriond, Les Arcs, France, 1982, edited by J. Tran Thanh Van (Editions, Frontiéres, Gif-sur-Yvette, 1982), p. 267; M. Tartaglia, Ph.D. thesis, Massachusetts Institute of Technology, 1984. Theoretical discussion of the process may be found in B. Kayser *et al.*, Phys. Rev. D **20**, 87 (1976).
[18]N. Ushida *et al.*, Phys. Rev. Lett. **47**, 1694 (1981) (E-531 at Fermilab).
[19]N. Ushida *et al.*, in *Proceedings of the XXIII International Conference on High Energy Physics,* Berkeley, California, 1986, edited by S. Loken (World Scientific, Singapore, 1987); N. Ushida *et al.*, Phys. Rev. Lett. **57**, 2897 (1986).
[20]A. E. Asratyan *et al.*, Phys. Lett. **105B**, 301 (1981).
[21]C. Angeline *et al.*, Phys. Lett. B **179**, 307 (1986).
[22]J. Blietschau *et al.*, Nucl. Phys. **B133**, 205 (1978) (GGM-PS Group at CERN).
[23]L. A. Ahrens *et al.*, Phys. Rev. D **31**, 2732 (1985).
[24]Several excellent reviews of the subject of neutrino oscillations are M. H. Shaevitz, in *Proceedings of the Oregon Meeting,* Annual Meeting of the Division of Particles and Fields of the APS, Eugene, 1985, edited by R. C. Hwa (World Scientific, Singapore, 1986), p. 426; K. E. Bergkvist, in *Proceedings of the 1985 International Symposium on Lepton and Photon Interactions at High Energies,* Kyoto, Japan, 1985, edited by M. Konuma and K. Takahashi (Research Institute for Fundamental Physics, Kyoto University, Kyoto, 1986).
[25]Neutrino oscillations may play an important role in the solar-neutrino problem. Renewed interest in the subject has been provoked by a suggestion of Mikeheyev and Smirnov. See H. A. Bethe, Phys. Rev. Lett. **56**, 1305 (1986).